

DTIC FILE COPY

REPORT SD-TR-88-99

④

## Ion Mixing of Ti and $TiO_y$ Films on $SiO_x$

Prepared by

A. A. GALUSKA, J. C. UHT, P. M. ADAMS and J. M. COGGI  
Materials Sciences Laboratory  
Laboratory Operations  
The Aerospace Corporation  
El Segundo, CA 90245

4 November 1988

Prepared for

SPACE DIVISION  
AIR FORCE SYSTEMS COMMAND  
Los Angeles Air Force Base  
P.O. Box 92960  
Los Angeles, CA 90009-2960

DTIC  
ELECTE  
DEC 20 1988  
S E D

APPROVED FOR PUBLIC RELEASE;  
DISTRIBUTION UNLIMITED

AD-A201 687

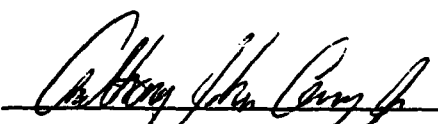
88 12 20 073

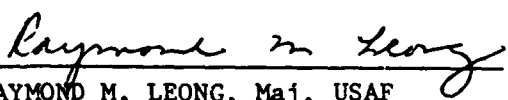
This report was submitted by The Aerospace Corporation, El Segundo, CA 90245, under Contract No. F04701-85-C-0086-P00016 with the Space Division, P.O. Box 92960, Los Angeles, CA 90009-2960. It was reviewed and approved for The Aerospace Corporation by R. W. Fillers, Director, Materials Sciences Laboratory.

Lt Constance M. Chintall/CNCIV was the project officer for the Mission-Oriented Investigation and Experimentation (MOIE) Program.

This report has been reviewed by the Public Affairs Office (PAS) and is releasable to the National Technical Information Service (NTIS). At NTIS, it will be available to the general public, including foreign nationals.

This technical report has been reviewed and is approved for publication. Publication of this report does not constitute Air Force approval of the report's findings or conclusions. It is published only for the exchange and stimulation of ideas.

  
for CONSTANCE M. CHINTALL, Lt, USAF  
MOIE Project Officer  
SD/CNCIV

  
RAYMOND M. LEONG, Maj, USAF  
Deputy Director, AFSTC West Coast Office  
AFSTC/WCO OL-AB

UNCLASSIFIED

SECURITY CLASSIFICATION OF THIS PAGE

## REPORT DOCUMENTATION PAGE

1a. REPORT SECURITY CLASSIFICATION Unclassified			1b. RESTRICTIVE MARKINGS		
2a. SECURITY CLASSIFICATION AUTHORITY			3. DISTRIBUTION/AVAILABILITY OF REPORT Approved for public release; distribution unlimited.		
2b. DECLASSIFICATION/DOWNGRADING SCHEDULE					
4. PERFORMING ORGANIZATION REPORT NUMBER(S) TR-0086A(2935-12)-4			5. MONITORING ORGANIZATION REPORT NUMBER(S) SD-TR-88-99		
6a. NAME OF PERFORMING ORGANIZATION The Aerospace Corporation Laboratory Operations		6b. OFFICE SYMBOL (if applicable)	7a. NAME OF MONITORING ORGANIZATION Space Division		
6c. ADDRESS (City, State, and ZIP Code) El Segundo, CA 90245			7b. ADDRESS (City, State, and ZIP Code) Los Angeles Air Force Base Los Angeles, CA 90009-2960		
8a. NAME OF FUNDING/SPONSORING ORGANIZATION		8b. OFFICE SYMBOL (if applicable)	9. PROCUREMENT INSTRUMENT IDENTIFICATION NUMBER F04701-85-C-0086 -P00016		
8c. ADDRESS (City, State, and ZIP Code)			10. SOURCE OF FUNDING NUMBERS		
		PROGRAM ELEMENT NO.	PROJECT NO.	TASK NO.	WORK UNIT ACCESSION NO.
11. TITLE (Include Security Classification) Ion Mixing of Ti and TiO <sub>y</sub> Films on SiO <sub>x</sub>					
12. PERSONAL AUTHOR(S) Galuska, A. A., Unt, J. C., Adams, P. M., and Coggi, J. M.					
13a. TYPE OF REPORT		13b. TIME COVERED FROM TO		14. DATE OF REPORT (Year, Month, Day) 1988 November 4	
15. PAGE COUNT 26					
16. SUPPLEMENTARY NOTATION					
17. COSATI CODES			18. SUBJECT TERMS (Continue on reverse if necessary and identify by block number)		
FIELD	GROUP	SUB-GROUP	Ion Implantation)		
			Interfacial Mixing,		
			Spectroscopy,		
			Xray Diffraction,		
			Titanium Oxide,		
			Silicon Oxide. <i>implant</i> ←		
19. ABSTRACT (Continue on reverse if necessary and identify by block number)					
<p>The influence of ion implantation on the interfacial chemistry, morphology, and adhesion of Ti and TiO<sub>y</sub> films on SiO<sub>x</sub> was examined. The Ti/SiO<sub>x</sub> and TiO<sub>y</sub>/SiO<sub>x</sub> specimens were implanted with varying doses of <sup>84</sup>Kr<sup>+</sup> at different substrate temperatures (2 × 10<sup>16</sup> Kr/cm<sup>2</sup> at 70°C, 1 × 10<sup>17</sup> Kr/cm<sup>2</sup> at 70°C, and 1 × 10<sup>17</sup> Kr/cm<sup>2</sup> at 350°C). These <sup>84</sup>Kr<sup>+</sup>-implanted specimens were compared to specimens vacuum annealed at 1000°C for 3600 s. Ion implantation intermixed interfacial Ti, Si, and O in both the Ti/SiO<sub>x</sub> and TiO<sub>y</sub>/SiO<sub>x</sub> specimens, producing interfacial Ti-Si oxide layers. This interfacial mixing increased with both implantation dose and</p>					
20. DISTRIBUTION/AVAILABILITY OF ABSTRACT <input checked="" type="checkbox"/> UNCLASSIFIED/UNLIMITED <input type="checkbox"/> SAME AS RPT. <input type="checkbox"/> DTIC USERS			21. ABSTRACT SECURITY CLASSIFICATION Unclassified		
22a. NAME OF RESPONSIBLE INDIVIDUAL			22b. TELEPHONE (Include Area Code)		22c. OFFICE SYMBOL

## 19. ABSTRACT (Continued)

temperature. Despite similar interfacial mixing, the influence of ion implantation on film adhesion was very different for the  $\text{Ti}/\text{SiO}_x$  and  $\text{TiO}_y/\text{SiO}_x$  specimens. Ion implantation promoted Si-O-Ti bonding at the  $\text{Ti}/\text{SiO}_x$  interface, resulting in a 10-fold adhesion increase. In contrast, ion implantation did not enhance the adhesion of the  $\text{TiO}_y$  films. The implanted  $^{84}\text{Kr}^+$  coalesced in both the  $\text{Ti}/\text{SiO}_x$  and  $\text{TiO}_y/\text{SiO}_x$  specimens, resulting in void, bubble, and crack formation. Film characterization was performed using Rutherford backscattering spectrometry, Auger electron spectroscopy, X-ray photoelectron spectroscopy, scanning electron microscopy, and X-ray diffraction. Film adhesion was examined using a scratch test.

# PREFACE

The authors are grateful to L. Crocko and S. Hornung for their assistance with the ion implantation and the AES/XPS analyses, respectively. The AES and XPS analyses were performed at the Analytical Service Center of the American Hospital Supply Corporation, Irvine, California. Ion implantation was performed at Kroko Engineering, Tustin, California. This work was supported by The Aerospace Corporation Mission Oriented Investigation and Experimentation program.

Accession For	
NTIS GRA&I	<input checked="" type="checkbox"/>
DTIC TAB	<input type="checkbox"/>
Unannounced	<input type="checkbox"/>
Justification	
By _____	
Distribution/	
Availability Codes	
Dist	Avail and/or Special
A-1	



## CONTENTS

I.	INTRODUCTION.....	7
II.	EXPERIMENTAL.....	9
III.	RESULTS AND DISCUSSION.....	11
IV.	SUMMARY/CONCLUSIONS.....	27
	REFERENCES.....	29

## FIGURES

1.	RBS Spectra of As-Deposited and Thermally Processed Ti/SiO <sub>x</sub> Specimens.....	12
2.	SEM Micrograph of a Ti/SiO <sub>x</sub> Specimen, Following Implan- tation with $1 \times 10^{17}$ Kr-cm <sup>-2</sup> at 70°C.....	13
3.	RBS Spectra of <sup>84</sup> Kr <sup>+</sup> -Implanted Ti/SiO <sub>x</sub> Specimens.....	15
4.	SEM Micrographs of Scratches Performed on As-Deposited and Ion-Processed Ti/SiO <sub>x</sub> Specimens.....	18
5.	RBS Spectra of As-Deposited and Annealed TiO <sub>y</sub> /SiO <sub>x</sub> Specimens.....	19
6.	SEM Micrograph of a TiO <sub>y</sub> /SiO <sub>x</sub> Specimen, Following Implantation with $1 \times 10^{17}$ Kr-cm <sup>-2</sup> at 70°C.....	20
7.	AES Depth Profiles of TiO <sub>y</sub> /SiO <sub>x</sub> Specimens Before and After Implantation with $1 \times 10^{17}$ Kr-cm <sup>-2</sup> at 350°C.....	22
8.	SEM Micrographs of Scratches Performed on Thermal and Ion-Processed TiO <sub>y</sub> /SiO <sub>x</sub> Specimens.....	25

## TABLES

1.	X-ray Diffraction Lines for Thermal and Ion-Processed Ti/SiO <sub>x</sub> .....	13
2.	Ti/SiO <sub>x</sub> Scratch Tests.....	16
3.	X-ray Diffraction Lines for Thermal and Ion-Processed TiO <sub>y</sub> /SiO <sub>x</sub> .....	21
4.	TiO <sub>y</sub> /SiO <sub>x</sub> Scratch Tests.....	23

## I. INTRODUCTION

Interfacial properties are often difficult to control using conventional deposition and thermal processing techniques. Ion mixing has potential for modifying these interfacial properties in previously unattainable ways.<sup>1-5</sup> In particular, ion mixing has been used rather extensively to enhance the adhesion between thin films and substrates. Ion mixing can increase thin film adhesion by inducing interfacial compound formation, by mechanically interlocking film and substrate, and by grading the interface between film and substrate.<sup>6-9</sup> Most investigations of ion-induced adhesion enhancement have dealt with metal films on oxide, polymer, semiconductor, and metal substrates.<sup>10-12</sup> Interfacial mixing, reaction, and adhesion enhancement are usually extensive when the film and substrate are exothermically reactive.<sup>11</sup> In contrast, interfacial mixing, reaction, and adhesion enhancement are usually minimal when the film and substrate are endothermically reactive.<sup>11,12</sup>

The potential of ion mixing for modifying the interfacial properties of metal oxide films on metal oxide substrates has yet to be adequately determined. The extent of ion-induced interfacial mixing is difficult to predict because most oxide-oxide reactions are neither highly exothermic nor highly endothermic. In addition, it is unclear whether ion mixing will promote the formation of glassy oxide mixtures or whether the oxide phases will separate. Both of these factors will have a large influence on the adhesion enhancement expected from ion mixing.

In this study, we investigated the influence of ion mixing on the interfacial properties of  $\text{TiO}_y$  and Ti films on  $\text{SiO}_x$ . The interactions of Ti and  $\text{TiO}_y$  with  $\text{SiO}_x$  are very different thermodynamically. The reduction-oxidation reaction between Ti and  $\text{SiO}_2$  is highly exothermic ( $2\text{Ti} + \text{SiO}_2 \rightarrow \text{Si} + 2\text{TiO}$ ;  $\Delta G_f^\circ = -167 \text{ kJ-mole}^{-1}$  at  $25^\circ\text{C}$ ). In contrast,  $\text{TiO}_2$  and  $\text{SiO}_2$  do not react to form a new product. They may be intermixed in a glassy form, but separate into discrete phases upon crystallization.<sup>13</sup> The ion-induced interfacial chemistry, morphology, and adhesion modifications produced in the Ti/ $\text{SiO}_x$  and  $\text{TiO}_y/\text{SiO}_x$  specimens are discussed in terms of the thermodynamic properties of the films.



## II. EXPERIMENTAL

The substrates used in our studies were n-type Czochralski silicon wafers with a  $\langle 100 \rangle$  orientation. The wafers were steam oxidized at 925°C to produce  $\text{SiO}_x$  ( $\text{SiO}_{2.2}$  as determined by Rutherford backscattering analysis) layers approximately 1300 Å thick. Prior to deposition the wafers were cleaned with trichloroethane, methanol, and deionized water. Titanium and titanium dioxide films 400 Å thick were deposited using magnetron sputtering with ultra-pure argon (99.999%) and a base pressure of  $5 \times 10^{-7}$  Torr. These films were implanted with  $^{84}\text{Kr}^+$  using a Varian Extrion 200-A2F ion implanter. The Extrion 200-A2F was equipped with a variable temperature stage heated by quartz halogen lamps. The samples were clipped to this implanter stage during implantation. Sample temperature was calibrated against stage temperature and the implant power density by placing iron-constantan thermocouples against the stage and the backside of a test sample during implantation at various power densities and stage temperatures. The  $^{84}\text{Kr}^+$  implants were performed using a 180 keV ion beam with a current density of  $2.5 \mu\text{A}\cdot\text{cm}^{-2}$ . Krypton implantation was performed at the following doses and temperatures:  $5 \times 10^{16} \text{ Kr}\cdot\text{cm}^{-2}$  at 70°C,  $1 \times 10^{17} \text{ Kr}\cdot\text{cm}^{-2}$  at 70°C, and  $1 \times 10^{17} \text{ Kr}\cdot\text{cm}^{-2}$  at 350°C. The ion beam energies were chosen in order to place the implantation peaks just beyond the critical interfaces.

Several of the as-deposited specimens were exposed to thermal treatments in order to compare the influence of thermal and ion processing. Thermal treatments were performed using a vacuum furnace. The furnace was pumped down to  $5 \times 10^{-7}$  Torr using an oil diffusion pump. The specimens were then heated to 1000°C for 3600 s.

The mixing process was examined using Rutherford backscattering spectroscopy (RBS) and Auger electron spectroscopy (AES). The RBS measurements were obtained on a General Ionex Tandetron Model 4110A using 3.0 MeV  $\text{He}^{++}$  ions. Specimens were tilted by 70° to improve depth resolution. AES analyses were obtained from a Perkin-Elmer PHI Multiprobe 6000 scanning Auger spectrometer using a 5.0 keV electron beam. Sputter depth profiling was performed using a 3.0 keV  $\text{Ar}^+$  ion beam. Crystallite identification was determined using X-ray

diffraction (XRD) with a Read camera (glancing  $15^\circ$  angle) and Cu  $K\alpha$  radiation. The diffracted X-ray intensities were very low. As a result, X-ray exposures of  $5.76 \times 10^4$  s were required. Analysis was performed under vacuum ( $\sim 1 \times 10^{-3}$  Torr) to minimize atmospheric scattering of the diffracted radiation. The chemical state of the films was examined with a Perkin-Elmer PHI 5400 X-ray photoelectron spectrometer (XPS) using Mg  $K\alpha$  radiation. The C 1s peak of adventitious carbon was used for energy calibration. This calibration gave Si 2p peaks at 103.3 and 99.0 eV for  $\text{SiO}_2$  and metallic Si, respectively. Sputter erosion and cleaning was performed using a 1 keV  $\text{Ar}^+$  ion beam. Ion sputtering resulted in the reduction of the  $\text{TiO}_2$  films to TiO and  $\text{Ti}_2\text{O}_3$ , but had no apparent influence on the  $\text{SiO}_2$  films.<sup>14</sup> Topographical changes and corresponding elemental compositions were determined using a Jeol JSM-840 scanning electron microscope (SEM) equipped with a Philips EDAX 9900 energy dispersive X-ray (EDX) system.

The adherence of the as-deposited and processed films was examined using a scratch test.<sup>15,16</sup> Scratch testing was performed on a Wilson Instruments Tukon microhardness tester using a  $136^\circ$  Knoop diamond indenter. Loads between 1 and 200 grams were applied to the indenter, which was manually drawn across the sample surface at  $\sim 0.2 \text{ mm-s}^{-1}$ . The minimum load necessary to remove a film from its substrate was used as a measure of the film adhesion. Scratches were examined by SEM to determine at what loads the films began to detach. EDX analysis was used to confirm the complete removal of the films from the scratches. The precision of these measurements was approximately 20% relative standard deviation for loads above 10 g.

### III. RESULTS AND DISCUSSION

#### A. Ti/SiO<sub>x</sub>/Si

The as-deposited Ti films were composed of  $\alpha$ - and  $\beta$ -Ti (see Fig. 1), and appeared smooth under SEM examination at 20,000X magnification. The RBS spectrum in Fig. 1a shows that the interface between the Ti and SiO<sub>x</sub> was discrete. The Ti films contained high concentrations of oxygen, which were incorporated during deposition and subsequent exposure to atmosphere. This oxygen concentration varied from ~ 47 atomic percent at the surface to ~ 16 atomic percent at the Ti/SiO<sub>x</sub> interface. As shown in Fig. 1b, vacuum annealing at 1000°C for 3600 s enhanced the reduction of the SiO<sub>x</sub> by the Ti film. The solubility of O in crystalline Ti is rather high (~ 30 atomic percent). As a result, the oxygen that was liberated from the SiO<sub>x</sub> layer was able to diffuse throughout the entire Ti film. Silicon, which diffuses very slowly in SiO<sub>2</sub> and is insoluble in crystalline TiO<sub>2</sub>, showed no redistribution upon annealing. XRD analysis (see Table 1) of the annealed specimens showed the presence of monoclinic TiO. The surface topography of the as-deposited specimens was unaffected by the anneal.

Ti/SiO<sub>x</sub> specimens were implanted with  $^{84}\text{Kr}^+$  to determine the influence of ion dose and implantation temperature on specimen chemistry and morphology. Krypton implants were performed to  $2 \times 10^{16}$  Kr-cm<sup>-2</sup> at 70°C,  $1 \times 10^{17}$  Kr-cm<sup>-2</sup> at 70°C, and  $1 \times 10^{17}$  Kr-cm<sup>-2</sup> at 350°C. The  $2 \times 10^{16}$  Kr-cm<sup>-2</sup> implant had no influence on the surface topography of the Ti/SiO<sub>x</sub> specimens. Increasing the dose to  $1 \times 10^{17}$  Kr-cm<sup>-2</sup> resulted in krypton coalescence in the SiO<sub>x</sub> layers. This coalescence produced a high density of voids and also surface bubbles on these  $^{84}\text{Kr}^+$  implanted specimens. An example of this voided surface topography is shown in Fig. 2. Implantation temperature had no influence on the observed surface topography.

RBS spectra of the  $^{84}\text{Kr}^+$ -implanted specimens are compared in Fig. 3. These RBS spectra show that approximately 50% of the implanted  $^{84}\text{Kr}^+$  passed through the Ti/SiO<sub>x</sub> interface. As with thermal processing, the  $2 \times 10^{16}$  Kr-cm<sup>-2</sup> implant enhanced the reduction of the SiO<sub>x</sub> layer and the diffusion of O throughout the Ti film. However, unlike thermal processing, ion bombardment

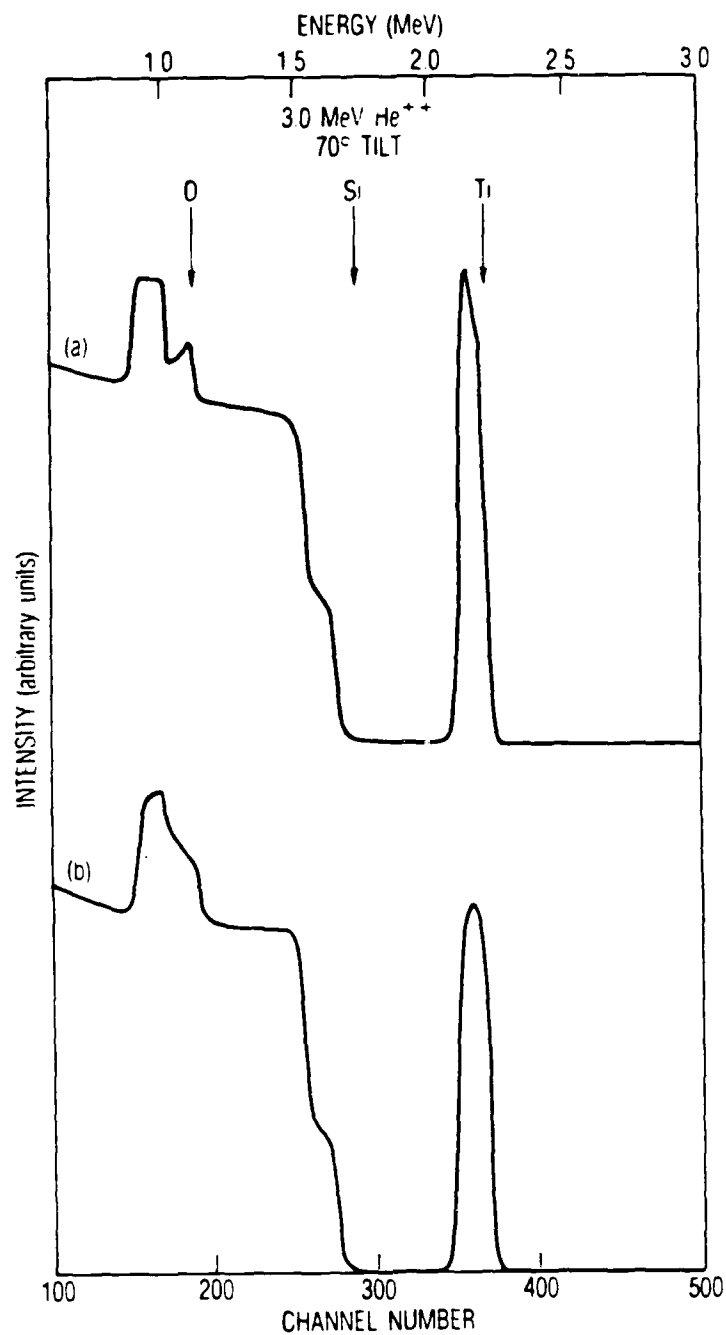


Fig. 1. RBS Spectra of As-Deposited and Thermally Processed Ti/SiO<sub>x</sub> Specimens. (a) As-Deposited specimen; (b) specimen vacuum annealed for 3600 s at 1000°C.

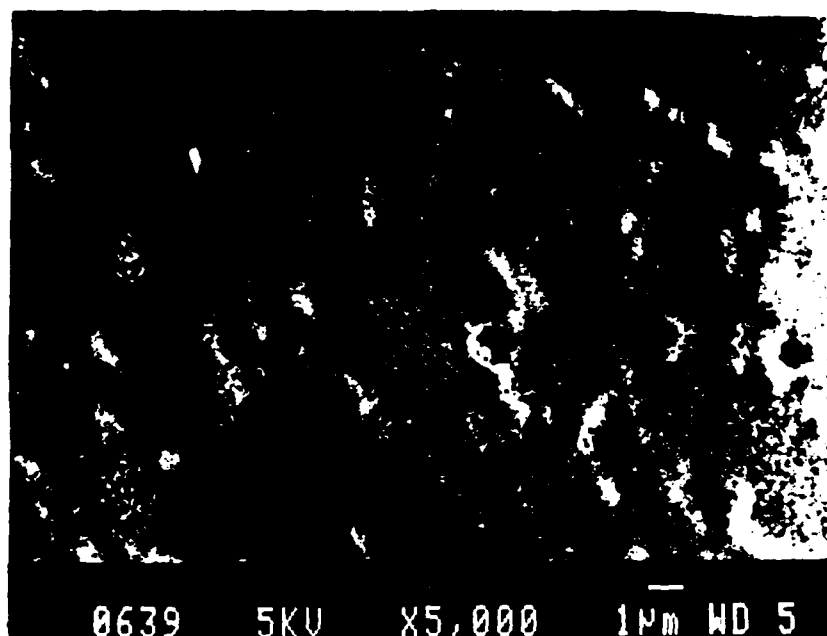


Fig. 2. SEM Micrograph of a  $\text{Ti/SiO}_x$  Specimen, Following Implantation with  $1 \times 10^{17} \text{ Kr-cm}^{-2}$  at  $70^\circ\text{C}$ . Micrometer sized bubbles and submicron sized voids are apparent.

also induced the intermixing of interfacial Si and Ti. The resulting Ti film had an average stoichiometry of approximately  $\text{TiO}_{0.9}\text{Si}_{0.3}$ . As expected for an ion-induced process, the gettering of O into the Ti film from the underlying  $\text{SiO}_x$  (also from the ambient above the specimen surface) increased substantially when the implant dose was increased to  $1 \times 10^{17} \text{ Kr-cm}^{-2}$  at  $70^\circ\text{C}$ . Similarly, the quantity of Ti mixed into the  $\text{SiO}_x$  layer increased with ion dose. In contrast, the quantity of Si mixed into the Ti film decreased. Ion mixing had lowered the miscibility of Si in the Ti film. This trend continued as the implantation temperature was increased to  $350^\circ\text{C}$ . As shown in Fig. 3d, the rise in temperature increased the gettering of O into the Ti film and the redistribution of Ti into the  $\text{SiO}_x$  underlayer. However, the Si content (also the Kr content) of the Ti film decreased. These elemental redistributions transformed the Ti film into  $\text{TiO}_{2.3}$  and the  $\text{SiO}_x$  layer into a mixed Ti-Si oxide layer, grading from the Si substrate to the  $\text{TiO}_{2.3}$  film. In addition to  $\text{Ti/SiO}_x$  intermixing, a small quantity of the implanted  $^{84}\text{Kr}^+$  reached the  $\text{SiO}_x/\text{Si}$  interface, producing a graded O distribution at that interface.

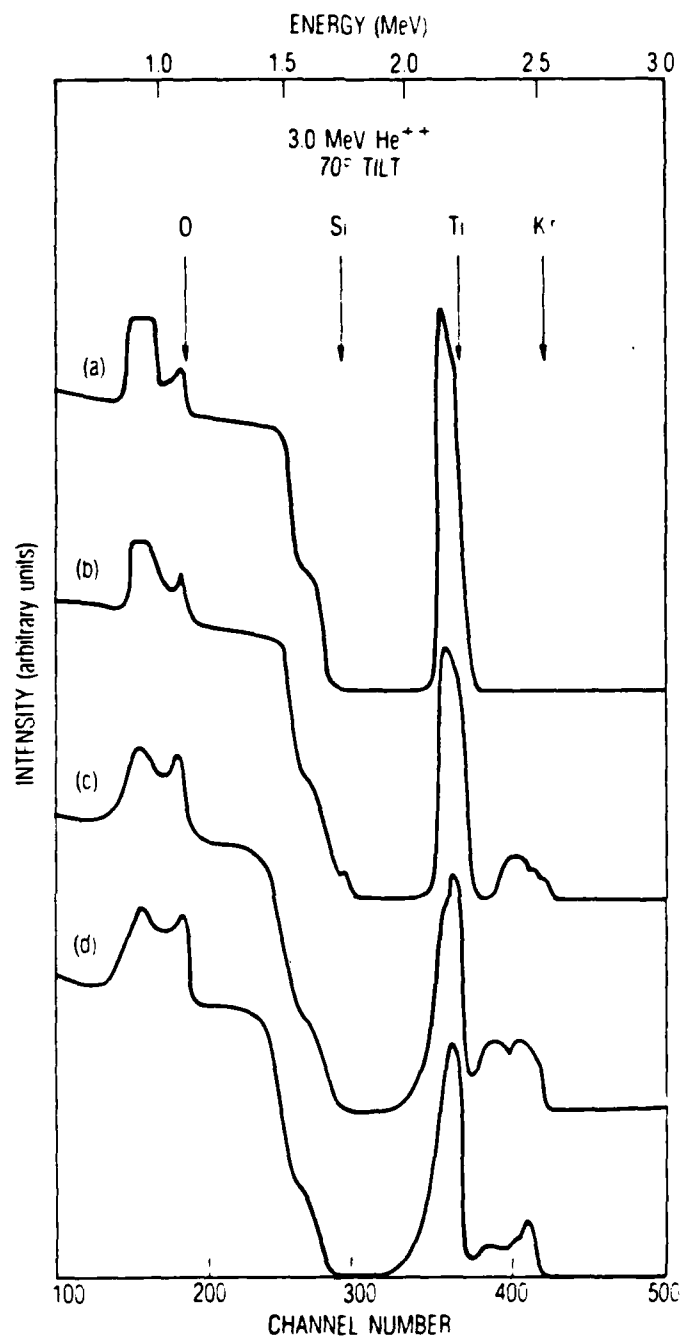


Fig. 3. RBS Spectra of  $^{84}\text{Kr}^+$ -Implanted  $\text{Ti/SiO}_x$  Specimens. (a) As-deposited specimen; (b) specimen implanted with  $2 \times 10^{16} \text{ Kr-cm}^{-2}$  at  $70^\circ\text{C}$ ; (c) specimen implanted with  $1 \times 10^{17} \text{ Kr-cm}^{-2}$  at  $70^\circ\text{C}$ ; (d) specimen implanted with  $1 \times 10^{17} \text{ Kr-cm}^{-2}$  at  $350^\circ\text{C}$ .

The chemical bonding produced in these ion-mixed Ti/SiO<sub>x</sub> specimens was examined using XRD and XPS analyses. As shown in Table 1, monoclinic TiO was the primary crystalline form produced by all of the <sup>84</sup>Kr<sup>+</sup> implants. The specimens implanted with 1 × 10<sup>17</sup> Kr-cm<sup>-2</sup> gave additional diffraction lines corresponding to more highly oxidized crystalline forms (TiO<sub>2</sub> and Ti<sub>3</sub>O<sub>5</sub>). This increased oxidation and crystallization explains why the intermixed Si was expelled from the Ti films during high dose implantation. Si is insoluble in crystalline TiO<sub>2</sub>.<sup>13,17</sup> Therefore, the solubility of Si in the Ti films decreased with ion-induced oxidation and crystallization. Any intermixed Si was driven out of the oxidized Ti films into the more highly disordered Ti-Si oxide films. The Kr content of the Ti films was also reduced as the films became more highly ordered.

Table 1. X-ray Diffraction Lines for Thermal and Ion-Processed Ti/SiO<sub>x</sub>

As-deposited d(Å)/I	Vacuum Annealed d(Å)/I	2 × 10 <sup>16</sup> Kr-cm <sup>-2</sup> , 70°C d(Å)/I	1 × 10 <sup>17</sup> Kr-cm <sup>-2</sup> , 70°C d(Å)/I	1 × 10 <sup>17</sup> Kr-cm <sup>-2</sup> , 350°C d(Å)/I
2.33/100 <sup>a</sup>	3.57/8 <sup>c</sup>	3.66/8 <sup>c</sup>	3.59/20 <sup>c,d</sup>	3.63/30 <sup>c,e</sup>
2.24/50 <sup>b</sup>	2.49/12 <sup>c</sup>	3.47/8 <sup>c</sup>	3.41/30 <sup>c</sup>	3.31/90 <sup>c,e</sup>
	2.38/12 <sup>c</sup>	2.44/100 <sup>c</sup>	2.38/30 <sup>c,d</sup>	2.68/50 <sup>e</sup>
	2.11/100 <sup>c</sup>	2.07/50 <sup>c</sup>	2.28/100 <sup>d</sup>	2.04/100 <sup>c</sup>
		1.48/20 <sup>c</sup>	2.04/100 <sup>c,d</sup>	1.68/30 <sup>c,e</sup>
			1.49/12 <sup>c</sup>	1.46/30 <sup>c</sup>

<sup>a</sup>Hexagonal β-Ti, calculated.

<sup>b</sup>Hexagonal α-Ti, PDF #5-0682.

<sup>c</sup>Monoclinic TiO, PDF #23-1078.

<sup>d</sup>Tetragonal TiO<sub>2</sub> (anatase), PDF #21-1273.

<sup>e</sup>Monoclinic Ti<sub>3</sub>O<sub>5</sub>, PDF #11-217.

The mixed Ti-Si oxide layers produced in the  $^{84}\text{Kr}^+$ -implanted specimens were examined using XPS. XPS analyses performed after sputter erosion into the mixed oxide layer showed a single broad Si 2p peak at 102.6 eV, characteristic of partially oxidized silicon ( $\sim \text{SiO}$ ). Silicon monoxide is a non-crystalline metastable phase, which decomposes to form Si and  $\text{SiO}_2$ .<sup>18,19</sup> The presence of partially oxidized Si, rather than separate  $\text{SiO}_2$  and Si phases, indicates that this Ti-Si oxide layer was a glassy mixture. Such a glass contains a high density of Si-O-Ti bonds.<sup>13</sup> The chemical state of the Ti in this mixed oxide layer could not be accurately determined by XPS analysis because of the chemistry modifications induced in titanium oxides by ion sputtering.

The adhesion between Ti and  $\text{SiO}_x$  in both the ion implanted and annealed Ti/ $\text{SiO}_x$  specimens was examined using a scratch test. The results of these scratch tests are summarized in Table 2. The adhesion values observed for the as-deposited, annealed, and ion-mixed specimens correlate with the extent of interfacial mixing and reaction (Si-O-Ti bond formation). The as-deposited Ti/ $\text{SiO}_x$  specimens had discrete interfaces, which showed little indication of reaction. These as-deposited films were weakly adherent, requiring only 5 g loads for removal. SEM/EDX analysis showed that the films were removed by brittle fracture at the Ti/ $\text{SiO}_x$  interface. We attribute this failure mode to stress concentration at the discrete Ti/ $\text{SiO}_x$  interfaces. An example of this

Table 2. Ti/ $\text{SiO}_x$  Scratch Tests

Sample Preparation	Load (g)	Sample Preparation	Load (g)
As-deposited	5 <sup>a</sup>	$2 \times 10^{16} \text{ Kr-cm}^{-2}$ , 70°C	15 <sup>b</sup>
		$1 \times 10^{17} \text{ Kr-cm}^{-2}$ , 70°C	50 <sup>b</sup>
Vacuum Annealed	25 <sup>b</sup>	$1 \times 10^{17} \text{ Kr-cm}^{-2}$ , 350°C	50 <sup>b</sup>

<sup>a</sup>Brittle interfacial fracture.

<sup>b</sup>Gradual thinning.



brittle interfacial failure is shown in Fig. 4a. The transfer of O into the Ti films, during thermal and low dose ion mixing, resulted in 3 to 5 fold adhesion increases. We attribute these adhesion increases to increases in Si-O-Ti bonding. The intermixing of the Ti and SiO<sub>x</sub> layers by high-dose ion implantation further enhanced this Si-O-Ti bonding. This Ti-SiO<sub>x</sub> intermixing increased film adhesion to 10 times that of the as-deposited specimens. As shown in Fig. 4b, film removal in the annealed and ion-mixed Ti/SiO<sub>x</sub> specimens occurred through gradual thinning, rather than brittle interfacial failure. We attribute this change in failure mode to interfacial grading. The abrupt change in materials properties at a discrete interface promotes abrupt interfacial fracture under scratch testing. However, the gradual change in materials properties at a graded interface promotes interfacial deformation, rather than fracture. With a more gradual film removal mechanism, such thinning would be expected.

#### B. TiO<sub>y</sub>/SiO<sub>x</sub>/Si

The as-deposited TiO<sub>y</sub> films were amorphous (examination by XRD) and smooth under SEM examination at 20,000X magnification. RBS analysis, presented in Fig. 5a, showed that the film stoichiometry was approximately TiO<sub>3</sub> and that the TiO<sub>y</sub>/SiO<sub>x</sub> interface was discrete. Vacuum annealing at 1000°C for 3600 s resulted in film crystallization to tetragonal TiO<sub>2</sub> (anatase). Grains 1 to 2 μm in diameter were observed under SEM examination. The RBS profile in Fig. 5b shows that vacuum annealing had no influence on the Ti and Si distributions. Crystalline TiO<sub>2</sub> and SiO<sub>2</sub> are immiscible.<sup>13,17</sup> However, oxygen, which is highly soluble (~ 30 atomic percent) in crystalline TiO<sub>2</sub> and SiO<sub>2</sub>, migrated from the TiO<sub>y</sub> layer to the Si/SiO<sub>x</sub> interface, resulting in SiO<sub>2</sub> growth.

As-deposited TiO<sub>y</sub>/SiO<sub>x</sub> specimens were implanted with <sup>84</sup>Kr<sup>+</sup> to 2 × 10<sup>16</sup> Kr-cm<sup>-2</sup> at 70°C, 1 × 10<sup>17</sup> Kr-cm<sup>-2</sup> at 70°C, and 1 × 10<sup>17</sup> Kr-cm<sup>-2</sup> at 350°C to determine the influence of ion dose and implantation temperature on specimen chemistry. The 2 × 10<sup>16</sup> Kr-cm<sup>-2</sup> implant had no influence on specimen topography or crystallinity. RBS analysis showed that the TiO<sub>y</sub>/SiO<sub>x</sub> interface had been slightly graded. A small quantity of Si (1.5 atomic percent) was mixed into the TiO<sub>y</sub> layer.

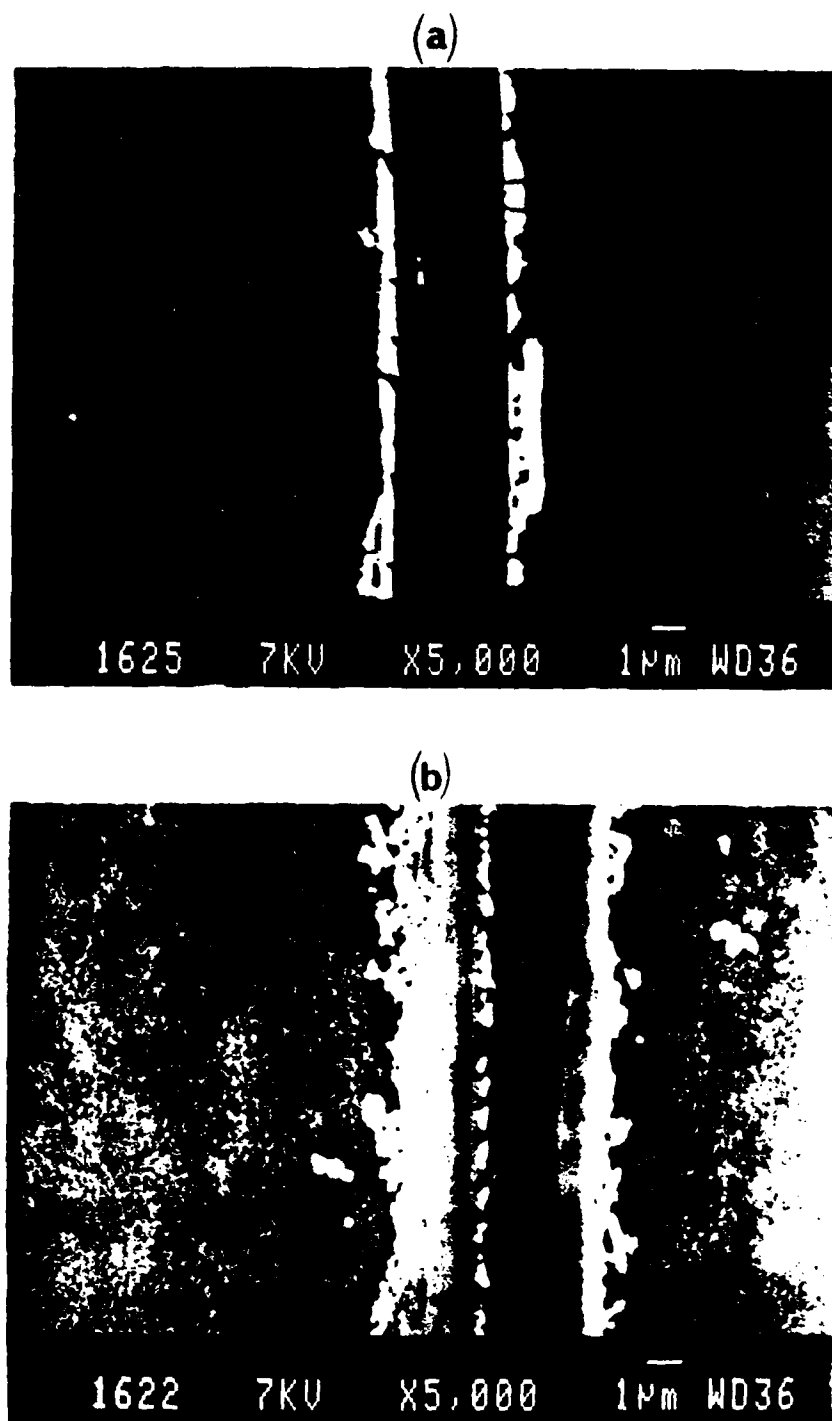


Fig. 4. SEM Micrographs of Scratches Performed on As-Deposited and Ion-Processed  $\text{Ti/SiO}_x$  Specimens. (a) 10 g scratch on as-deposited specimen; (b) 50 g scratch on specimen implanted with  $1 \times 10^{17} \text{ Kr-cm}^{-2}$  at  $70^\circ\text{C}$ .

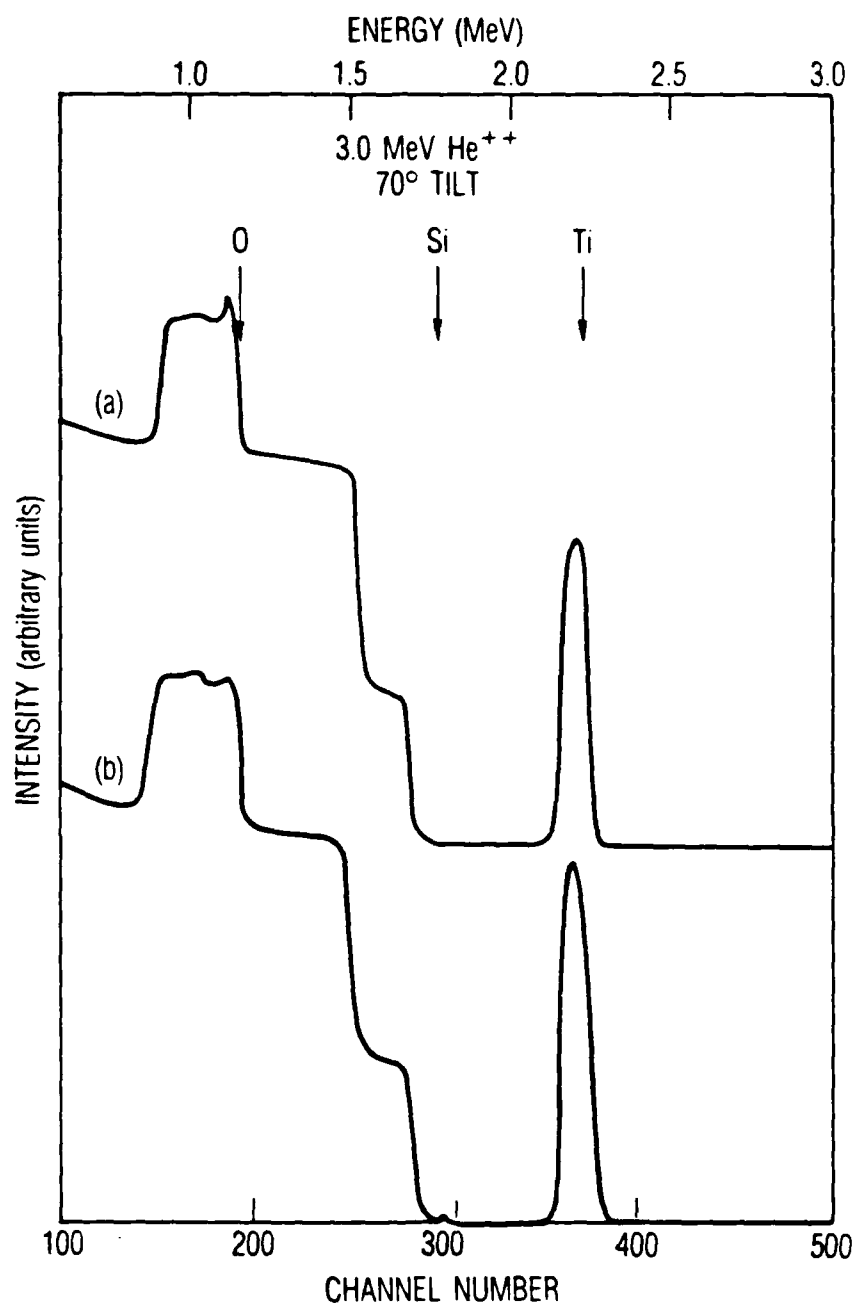


Fig. 5. RBS Spectra of As-Deposited and Annealed  $\text{TiO}_y/\text{SiO}_x$  Specimens. (a) As-deposited specimen; (b) Specimen vacuum annealed at 1000°C for 3600 s.

The  $1 \times 10^{17}$  Kr-cm<sup>-2</sup> implants, performed at both 70 and 350°C, caused the TiO<sub>y</sub> films to fracture into platelets 1 to 5 μm in diameter. The implanted Kr coalesced in the SiO<sub>x</sub> films to form a high density of submicron-sized voids, resulting in film expansion. SiO<sub>x</sub> expansion induced tensile stresses in the TiO<sub>y</sub> films. The TiO<sub>y</sub> films, which have much lower ductility than the Ti films, fractured under these tensile stresses, producing the platelet structure shown in Fig. 6. The voids produced by krypton coalescence are readily apparent in the cracks between the platelets, but are absent from the platelets.

AES depth profiles were obtained from the platelet and crack regions of these high-dose TiO<sub>y</sub>/SiO<sub>x</sub> specimens. Depth profiles performed in the platelet regions exhibited substantial grading at the TiO<sub>y</sub>/SiO<sub>x</sub> interface, much like

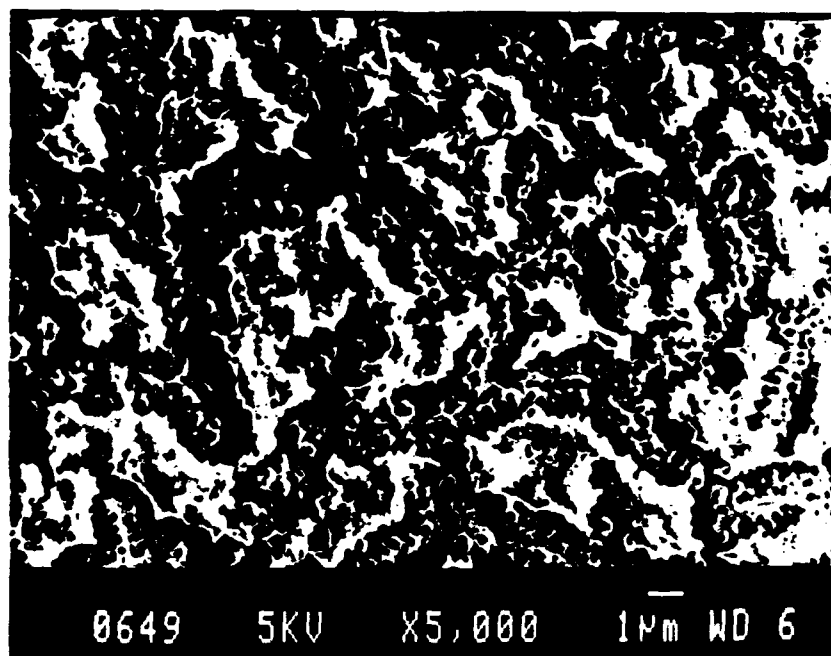


Fig. 6. SEM Micrograph of a TiO<sub>y</sub>/SiO<sub>x</sub> Specimen, Following Implantation with  $1 \times 10^{17}$  Kr-cm<sup>-2</sup> at 70°C. The surface, which was initially smooth, was transformed into a series of cracks and platelets. A high density of voids is observed in the crack regions.

that observed in the ion-mixed  $\text{Ti/SiO}_x$  specimens. The quantity of Ti mixed into the  $\text{SiO}_x$  layers increased with ion dose and temperature, but the quantity of Si in the  $\text{TiO}_y$  layers decreased with ion dose and temperature. The interfacial mixing induced by the  $1 \times 10^{17} \text{ Kr-cm}^{-2}$  implant performed at  $350^\circ\text{C}$  is shown in Fig. 7b. The Ti distribution extends completely through the  $\text{SiO}_x$  layer. The Si distribution extends partially into the  $\text{TiO}_y$ , but leaves most of the  $\text{TiO}_y$  film intact. Depth profiles (Fig. 7c) obtained from the crack regions did not exhibit this  $\text{TiO}_y$  layer. The cracks were composed of an intermixed layer of Ti, Si, and O, which was graded into the Si substrate. This mixed composition verified that the cracks had originated from the intermixed  $\text{TiO}_y/\text{SiO}_x$  interface.

The chemistry of these ion-mixed  $\text{TiO}_y/\text{SiO}_x$  specimens was examined using XRD and XPS analyses. The X-ray diffraction patterns (presented in Table 3), obtained from the specimens implanted with high  $^{84}\text{Kr}^+$  doses, showed that the  $\text{TiO}_y$  surfaces had crystallized to tetragonal  $\text{TiO}_2$  (both rutile and anatase). The absence of any reduced crystalline forms ( $\text{TiO}$ ,  $\text{Ti}_2\text{O}_3$ , etc.) indicates that the  $\text{TiO}_y$  film had crystallized with a high degree of perfection. As with the ion-mixed  $\text{Ti/SiO}_x$  specimens, this crystallization forced defects (such as intermixed Si and coalesced Kr) out of the  $\text{TiO}_2$  films. The absence of partially oxidized crystalline forms also indicates that the Ti in the Ti-Si oxide layer had one distinct form. It was present in either a glassy mixture (no diffraction pattern) or in a crystalline  $\text{TiO}_2$  phase. XPS spectra taken from these mixed oxide layers exhibited a single Si 2p peak at 103.3 eV, characteristic of  $\text{SiO}_2$ . Such a peak would be observed from a separate  $\text{SiO}_2$  phase or a glassy mixture of  $\text{SiO}_2$  and  $\text{TiO}_2$ . It is unclear from the XRD and XPS analyses whether the intermixed region was composed of a glassy mixture, or separate  $\text{SiO}_2$  and  $\text{TiO}_2$  phases.

The results of adhesion tests performed on the as-deposited, annealed, and ion processed  $\text{TiO}_y/\text{SiO}_x$  specimens are summarized in Table 4. Ion mixing and annealing produced only small changes in the adhesion of the  $\text{TiO}_y$  films. The as-deposited films were removed at 25 g loads. Annealing at  $1000^\circ\text{C}$  for 3600 s reduced this critical load to 17 g. Film crystallization either increased the intrinsic stress at the interface, or enhanced the transfer of

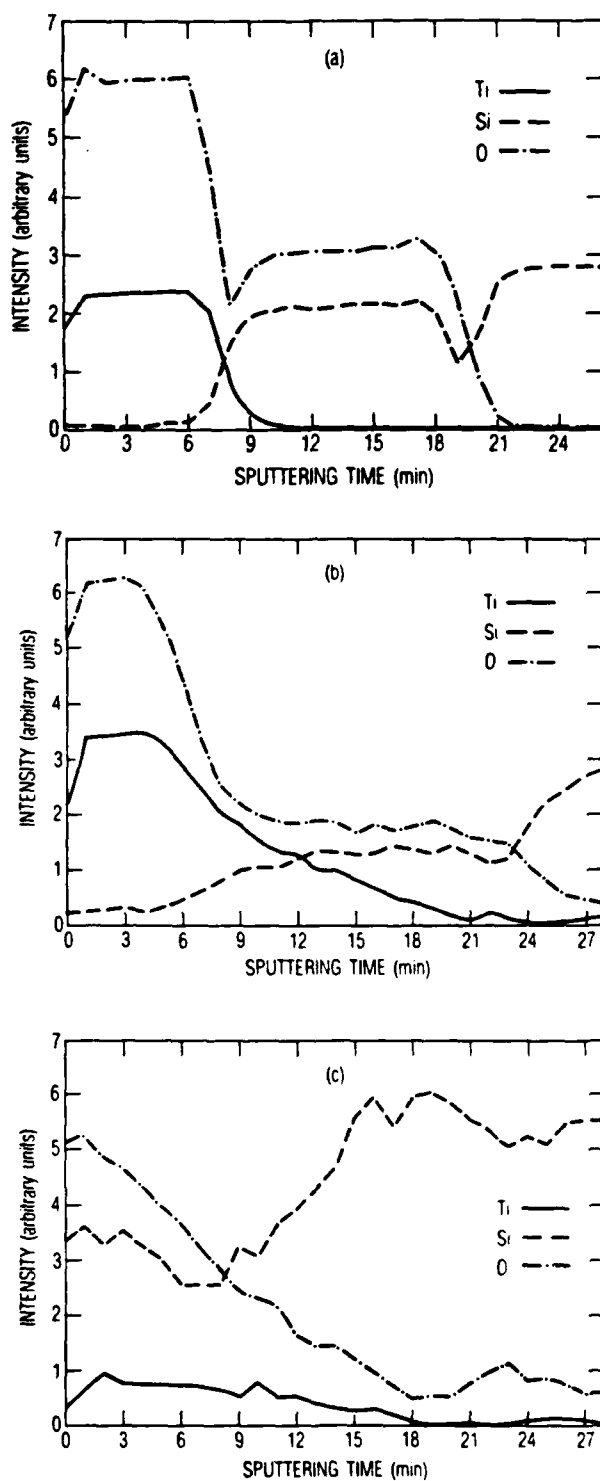


Fig. 7. AES Depth Profiles of  $\text{TiO}_y/\text{SiO}_x$  Specimens Before and After Implantation with  $1 \times 10^{17} \text{ Kr-cm}^{-2}$  at  $350^\circ\text{C}$ .  
 (a) As-deposited specimen; (b) Surface platelet on the implanted specimen; (c) Crack region between platelets on the implanted specimen.

Table 3. X-ray Diffraction Lines for Thermal and Ion-Processed  $\text{TiO}_y/\text{SiO}_x$

As-deposited $d(\text{\AA})/I$	Vacuum Annealed $d(\text{\AA})/I$	$2 \times 10^{16} \text{ Kr-cm}^{-2}$ , 70°C $d(\text{\AA})/I$	$1 \times 10^{17} \text{ Kr-cm}^{-2}$ , 70°C $d(\text{\AA})/I$	$1 \times 10^{17} \text{ Kr-cm}^{-2}$ , 350°C $d(\text{\AA})/I$
No Lines Observed	3.65/100 <sup>a</sup> 2.48/20 <sup>a,b</sup> 1.97/20 <sup>a</sup> 1.76/20 <sup>a</sup>	No Lines Observed	3.66/8 <sup>a</sup> 3.22/100 <sup>b</sup> 2.30/8 <sup>b</sup>	3.21/100 <sup>b</sup> 2.50/30 <sup>a,b</sup> 1.69/30 <sup>b</sup>

<sup>a</sup>Tetragonal  $\text{TiO}_2$  (anatase), PDF #21-1273.

<sup>b</sup>Tetragonal  $\text{TiO}_2$  (rutile), PDF #21-1276.

Table 4.  $\text{TiO}_y/\text{SiO}_x$  Scratch Tests

Sample Preparation	Load (g)	Sample Preparation	Load (g)
As-deposited	25 <sup>a</sup>	$2 \times 10^{16} \text{ Kr-cm}^{-2}$ , 70°C	10 <sup>b</sup>
		$1 \times 10^{17} \text{ Kr-cm}^{-2}$ , 70°C	30 <sup>b</sup>
Vacuum Annealed	17 <sup>a</sup>	$1 \times 10^{17} \text{ Kr-cm}^{-2}$ , 350°C	30 <sup>b</sup>

<sup>a</sup>Brittle interfacial fracture.

<sup>b</sup>Gradual thinning.

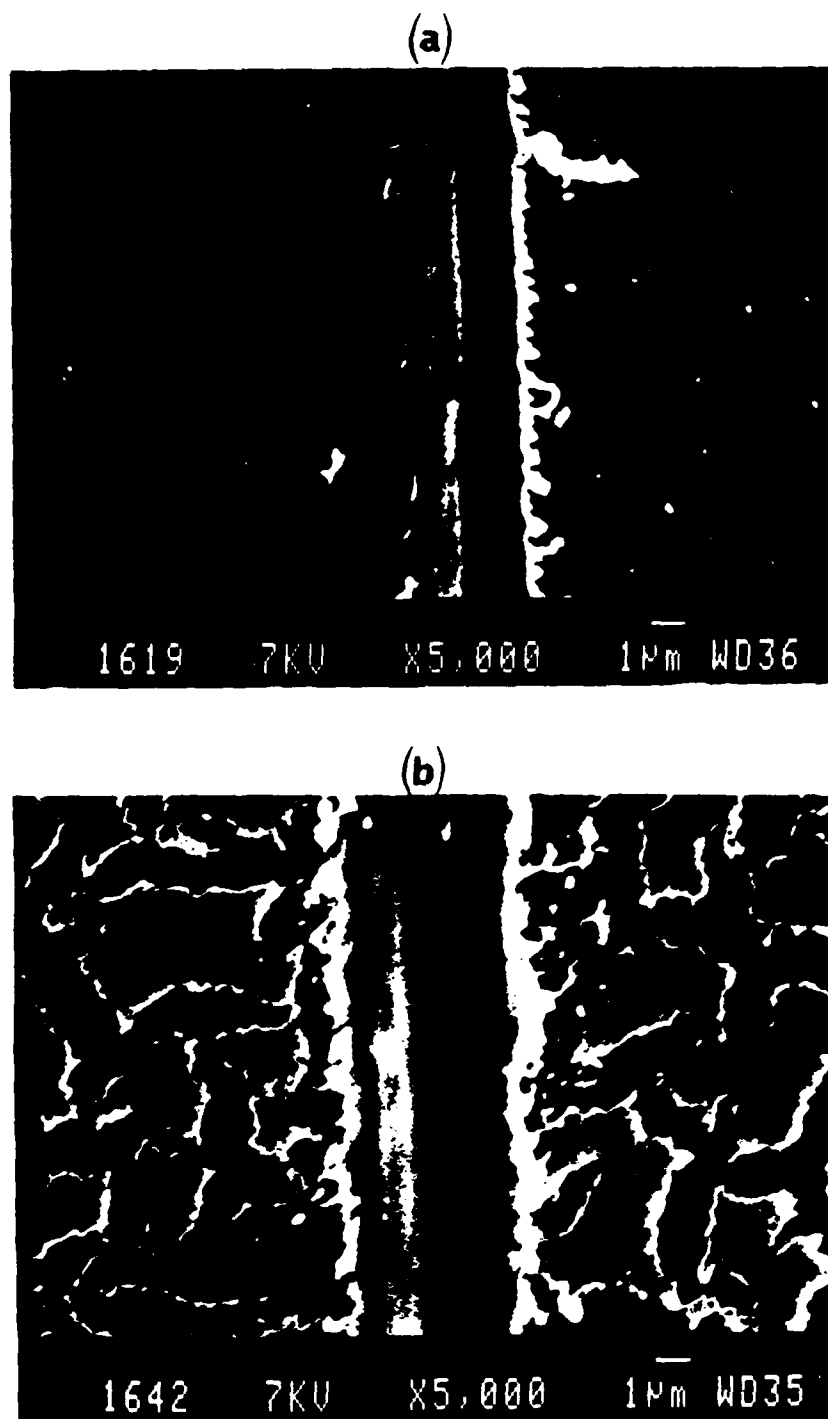


Fig. 8. SEM Micrographs of Scratches Performed on Thermal and Ion-Processed  $\text{TiO}_y/\text{SiO}_x$  Specimens. (a) 17 g scratch on specimen annealed at  $1000^\circ\text{C}$  for 3600 s; (b) 30 g scratch on specimen implanted with  $1 \times 10^{17} \text{ Kr-cm}^{-2}$  at  $70^\circ\text{C}$ .



applied stress to the interface. Both the as-deposited and annealed  $\text{TiO}_y$  films were removed through brittle interfacial fracture that resulted from stress concentration at the discrete  $\text{TiO}_y/\text{SiO}_x$  interfaces. An SEM micrograph of the brittle fracture induced by a 17 g scratch on a vacuum annealed  $\text{TiO}_y/\text{SiO}_x$  specimen is shown in Fig. 8a. The  $\text{TiO}_y$  films implanted with  $2 \times 10^{16} \text{ Kr-cm}^{-2}$  showed a reduction in adhesion to 10 g loads. Apparently, the interfacial stresses induced by ion implantation ( $\text{SiO}_x$  expansion) were far greater than any adhesion enhancement. For those specimens implanted with  $1 \times 10^{17} \text{ Kr-cm}^{-2}$ , ion-induced interfacial stresses were relieved by the fracturing of the  $\text{TiO}_y$  films. The loads required to remove these high-dose films remained approximately the same as the as-deposited films. As shown in Fig. 8b, the  $^{84}\text{Kr}^+$  implanted films were not removed by interfacial fracture, but were removed through a gradual thinning process. The gradual change in materials properties at the graded (ion-mixed)  $\text{TiO}_y/\text{SiO}_x$  interfaces promotes interfacial deformation, rather than fracture.

Although the  $\text{TiO}_y$  and  $\text{SiO}_x$  films were mechanically interlocked through ion mixing, the adhesion of the  $\text{TiO}_y$  films was not improved. Apparently, interfacial mixing was not accompanied by enhanced Si-O-Ti bonding across the  $\text{TiO}_y/\text{SiO}_x$  interface. The XRD data obtained from the ion mixed  $\text{TiO}_y/\text{SiO}_x$  specimens indicated that the form of the Ti in the mixed oxide layer was either glassy (extensive Si-O-Ti bonding) or highly crystalline (little Si-O-Ti bonding). We attribute the absence of ion-induced adhesion enhancement to  $\text{TiO}_2$  crystallization and phase separation in the interfacial Ti-Si oxide layer. However, a further investigation, including high energy electron diffraction, is required to verify this hypothesis.

#### IV. SUMMARY/CONCLUSIONS

Ion implantation induced interfacial mixing at both the  $\text{TiO}_y/\text{SiO}_x$  and the  $\text{Ti}/\text{SiO}_x$  interfaces. As with thermal processing, ion implantation enhanced the reduction-oxidation reaction between the Ti and  $\text{SiO}_x$  layers, resulting in O redistribution into the Ti films. Contrary to thermal processing, ion implantation induced the redistribution of Ti from the Ti and  $\text{TiO}_y$  films into the underlying  $\text{SiO}_x$  layers. Silicon was also ion mixed into the Ti and  $\text{TiO}_y$  films, but most of this intermixed Si was expelled because of the poor solubility of Si in crystalline  $\text{TiO}_2$ . Ion-induced interfacial mixing, which produced interfacial Ti-Si oxide layers in both the  $\text{Ti}/\text{SiO}_x$  and  $\text{TiO}_y/\text{SiO}_x$  specimens, increased with ion dose and implantation temperature.

Although ion implantation induced similar interfacial mixing in both the  $\text{TiO}_y/\text{SiO}_x$  and  $\text{Ti}/\text{SiO}_x$  specimens, ion implantation had a very different influence on the adhesion of the Ti and  $\text{TiO}_y$  films. The interfacial mixing (mechanical interlocking) induced by ion implantation enhanced the adhesion of the Ti films by 10-fold, but did not enhance the adhesion of the  $\text{TiO}_y$  films. The observed adhesion increases were attributed to increased Si-O-Ti bonding. Because of the low O content of the Ti films, interfacial mixing in the  $\text{Ti}/\text{SiO}_2$  specimens inevitably produced greater Si-O-Ti bonding (adhesion enhancement). This was not true in the  $\text{TiO}_y/\text{SiO}_x$  specimens. In fact, XRD analyses indicate that the mixed Ti-Si oxide layers in the  $\text{TiO}_y/\text{SiO}_x$  specimens may have separated into discrete  $\text{TiO}_2$  and  $\text{SiO}_2$  phases.

The topography of the Ti and  $\text{TiO}_y$  films was also influenced differently by ion implantation. The coalescence of the implanted Kr induced  $\text{SiO}_x$  expansion. This expansion induced tensile stresses in both the Ti and  $\text{TiO}_y$  films. These stresses caused the brittle  $\text{TiO}_y$  films to fracture into platelets. The Ti films, which have greater ductility than the  $\text{TiO}_y$  films, did not fracture, but showed signs of plastic deformation.

From this investigation, it is clear that both metal/oxide and oxide/oxide interfaces may be mixed rather extensively by ion implantation. However, this interfacial mixing does not necessarily enhance adhesion. Increased chemical bonding across the interface is required for adhesion

improvement. As with the  $\text{TiO}_y/\text{SiO}_x$  specimens, this chemical bonding may not be observed between oxide layers that are not thermodynamically reactive. In addition, the high implantation doses required to intermix an oxide/oxide interface can result in substantial topographical damage, which is unacceptable for most thin film applications.

## REFERENCES

1. I. L. Singer, Appl. Surf. Sci. **18**, 28 (1984).
2. M. Van Rossum, M-A. Nicolet, and C. H. Wilts, J. Appl. Phys. **56**, 1032 (1984).
3. K. C. Cadien and J. E. Greene, Appl. Phys. Lett. **40**, 329 (1982).
4. J. W. Mayer and S. S. Lau, "Surface Modification and Alloying by Laser, Ion, and Electron Beams," edited by J. M. Poate, G. Foti, and D. C. Jacobson (Plenum, New York, 1983), p. 240.
5. S. Matteson and M-A. Nicolet, Ann. Rev. Mater. Sci. **13**, 339 (1983).
6. A. A. Galuska, J. Vac. Sci. Technol. B **5**, 1 (1987).
7. D. M. Mattox, "Adhesion Measurement of Thin Films, Thick Films, and Bulk Coatings," edited by K. L. Mittal (American Society for Testing and Materials, Philadelphia, 1978), p. 54.
8. I. V. Mitchell, J. S. Williams, D. K. Sood, K. T. Short, S. Johnson, and R. G. Elliman, in "Proceedings of MRS Symposium on Thin Films and Interfaces," edited by J. E. E. Baglin, D. R. Campbell, and W. K. Chu (North Holland, New York, 1984), p. 189.
9. J. E. E. Baglin and G. J. Clark, Nucl. Instrum. Methods Phys. Res. B **107**, 89 (1985).
10. S. Jacobson, B. Johnson and B. Sunquist, Thin Solid Films **107**, 89 (1983).
11. C. W. White, G. Farlow, J. Narayan, G. J. Clark, and J. E. E. Baglin, Mat. Lett. **2**, 367 (1984).
12. T. A. Tombrello, "Proceedings of MRS Symposium on Thin Films and Interfaces," edited by J. E. E. Baglin, D. R. Campbell, and W. K. Chu (North-Holland, New York, 1984), p. 179.
13. M. F. Best and R. A. Condrate, J. Mat. Sci. Lett. **4**, 994 (1985).
14. R. Kelly, "Ion Bombardment Modification of Surfaces," edited by O. Auciello and R. Kelly (Elsevier, New York, 1984), p. 85.
15. I. S. Goldstein and R. DeLong, J. Vac. Sci. Technol. **20**, 327 (1982).
16. B. N. Chapman, J. Vac. Sci. Technol. **11**, 106 (1947).
17. R. C. De Vries, R. Roy and E. F. Osborn, Trans. Brit. Ceram. Soc. **53**, 531 (1954).

18. R. B. Sosman, Trans. Brit. Ceram. Soc. 54, 655 (1955).
19. H. H. Emons and H. Boenicke, Wess. Z. Tech. Hochsch. Chem. Leuna-Merseburg 4, 115 (1961).

## LABORATORY OPERATIONS

The Aerospace Corporation functions as an "architect-engineer" for national security projects, specializing in advanced military space systems. Providing research support, the corporation's Laboratory Operations conducts experimental and theoretical investigations that focus on the application of scientific and technical advances to such systems. Vital to the success of these investigations is the technical staff's wide-ranging expertise and its ability to stay current with new developments. This expertise is enhanced by a research program aimed at dealing with the many problems associated with rapidly evolving space systems. Contributing their capabilities to the research effort are these individual laboratories:

Aerophysics Laboratory: Launch vehicle and reentry fluid mechanics, heat transfer and flight dynamics; chemical and electric propulsion, propellant chemistry, chemical dynamics, environmental chemistry, trace detection; spacecraft structural mechanics, contamination, thermal and structural control; high temperature thermomechanics, gas kinetics and radiation; cw and pulsed chemical and excimer laser development including chemical kinetics, spectroscopy, optical resonators, beam control, atmospheric propagation, laser effects and countermeasures.

Chemistry and Physics Laboratory: Atmospheric chemical reactions, atmospheric optics, light scattering, state-specific chemical reactions and radiative signatures of missile plumes, sensor out-of-field-of-view rejection, applied laser spectroscopy, laser chemistry, laser optoelectronics, solar cell physics, battery electrochemistry, space vacuum and radiation effects on materials, lubrication and surface phenomena, thermionic emission, photo-sensitive materials and detectors, atomic frequency standards, and environmental chemistry.

Computer Science Laboratory: Program verification, program translation, performance-sensitive system design, distributed architectures for spaceborne computers, fault-tolerant computer systems, artificial intelligence, microelectronics applications, communication protocols, and computer security.

Electronics Research Laboratory: Microelectronics, solid-state device physics, compound semiconductors, radiation hardening; electro-optics, quantum electronics, solid-state lasers, optical propagation and communications; microwave semiconductor devices, microwave/millimeter wave measurements, diagnostics and radiometry, microwave/millimeter wave thermionic devices; atomic time and frequency standards; antennas, rf systems, electromagnetic propagation phenomena, space communication systems.

Materials Sciences Laboratory: Development of new materials: metals, alloys, ceramics, polymers and their composites, and new forms of carbon; non-destructive evaluation, component failure analysis and reliability; fracture mechanics and stress corrosion; analysis and evaluation of materials at cryogenic and elevated temperatures as well as in space and enemy-induced environments.

Space Sciences Laboratory: Magnetospheric, auroral and cosmic ray physics, wave-particle interactions, magnetospheric plasma waves; atmospheric and ionospheric physics, density and composition of the upper atmosphere, remote sensing using atmospheric radiation; solar physics, infrared astronomy, infrared signature analysis; effects of solar activity, magnetic storms and nuclear explosions on the earth's atmosphere, ionosphere and magnetosphere; effects of electromagnetic and particulate radiations on space systems; space instrumentation.